Can spherical eukaryotic microalgae cells be treated as optically homogeneous?

ARKA BHOWMIK AND LAURENT PILON*

Mechanical and Aerospace Engineering Department, Henry Samueli School of Engineering and Applied Science, University of California, Los Angeles, 420 Westwood Plaza, Eng. IV 37-132, Los Angeles, California 90095, USA
*Corresponding author: pilon@seas.ucla.edu

This study aims to answer the question of whether spherical unicellular photoautotrophic eukaryotic microalgae cells, consisting of various intracellular compartments with their respective optical properties, can be modeled as homogeneous spheres with some effective complex index of refraction. The spectral radiation characteristics in the photosynthetically active region of a spherical heterogeneous microalgae cell, representative of *Chlamydomonas reinhardtii* and consisting of spherical compartments corresponding to the cell wall, cytoplasm, chloroplast, nucleus, and mitochondria, were estimated using the superposition T-matrix method. The effects of the presence of intracellular lipids and/or starch accumulation caused by stresses, such as nitrogen limitation, were explored. Predictions by the T-matrix method were qualitatively and quantitatively consistent with experimental measurements for various microalgae species. The volume-equivalent homogeneous sphere approximation with volume-averaged effective complex index of refraction gave accurate estimates of the spectral (i) absorption and (ii) scattering cross sections of the heterogeneous cells under both nitrogen-replete and nitrogen-limited conditions. In addition, the effect of a strongly refracting cell wall, representative of *Chlorella vulgaris*, was investigated. In this case, for the purpose of predicting their integral radiation characteristics, the microalgae should be represented as a coated sphere with a coating corresponding to the cell wall and a homogeneous core with volume-averaged complex index of refraction for the rest of the cell. However, both homogeneous sphere and coated sphere approximations predicted strong resonances in the scattering phase function and spectral backscattering cross section that were not observed in that of the heterogeneous cells.   © 2016 Optical Society of America

OCIS codes: (010.5620) Radiative transfer; (290.7050) Turbid media; (010.1030) Absorption; (290.0290) Scattering; (010.1350) Backscattering.

http://dx.doi.org/10.1364/JOSAA.33.001495

1. INTRODUCTION

Estimating the absorption and scattering cross sections, the scattering phase function and the backscattering ratio of photosynthetic eukaryotic microalgae cells have been a subject of interest in various fields, including ocean optics for real-time monitoring of algal blooms using satellite remote sensing [1–3], biofuel production [4–6], and biomass production of value-added products [7]. In remote sensing of microalgae blooms, the objective is to monitor and detect the blooms by comparing the spatial and temporal changes in chlorophyll *a* (Chl *a*) concentration maps [8]. The latter are constructed by fitting the measured spectral reflectance with a theoretical model accounting for the dependency of microalgae's radiation characteristics on their Chl *a* concentration [8–10]. On the other hand, predicting and controlling light transfer through microalgae suspensions in photobioreactors (PBRs) is essential to maximize the productivity of lipid, hydrogen, and other

value-added products, such as food supplements and coloring agents [11–14]. Several models have been developed to relate light transfer to microalgae growth kinetics in PBRs [15–17]. Overall, light transfer models used in the above-mentioned applications are based on some solution of the radiative transfer equation and require knowledge of the radiation characteristics of the microalgae species of interest.

Estimating the radiation characteristics of eukaryotic cells is challenging due to their heterogeneous and nonspherical structures [1,18,19] and by the limited knowledge of the spectral optical properties of intracellular organelles [1]. In spite of their heterogeneous nature, microalgae cells have commonly been approximated as homogeneous spheres with some effective complex index of refraction for predicting their radiation characteristics [1–3,16,20–24]. This approximation can be justified, *a priori*, based on the small mismatch in complex index of refraction among the organelles within the cell. Pottier *et al.* [16] predicted the radiation characteristics of

Chlamydomonas reinhardtii, based on the Lorenz–Mie theory, by treating them as spherical homogeneous cells with some effective complex index of refraction. The effective absorption index $k_{\lambda,\mathrm{eff}}$ of each cell was expressed as a concentration-weighted sum of the pigments' specific spectral absorption coefficients while their refractive index was taken as constant over the photosynthetically active radiation (PAR) region [16]. More recently, Dauchet *et al.* [22] recommended the use of a wavelength-dependent effective refractive index $n_{\lambda,\mathrm{eff}}$ determined from the effective absorption index $k_{\lambda,\mathrm{eff}}$ based on the subtractive Kramers–Kronig relation.

Alternatively, Quirantes and Bernard [21] approximated microalgae cells as coated spheres such that the outer coating assumed the spectral optical properties n_λ and k_λ of the chloroplast while the inner core had some effective optical properties $n_{\mathrm{eff},\lambda}$ and $k_{\mathrm{eff},\lambda}$ representative of the cytoplasm and other organelles in the PAR region of the spectrum, between 400 and 700 nm. The coated sphere approximation was found to be superior to the homogeneous sphere approximation for retrieving the spectral optical properties of microalgae.

Moreover, Svensen *et al.* [25] measured the scattering phase function of *C. reinhardtii* cells with and without cell wall grown under optimal growth conditions. The results indicated that the measured scattering phase function in the forward direction for cells with or without a wall were nearly identical. However, cells with a wall featured a larger scattering coefficient and backscattering ratio than wall-less cells. The authors also compared qualitatively the measured phase functions with those computed by the Lorenz–Mie theory for coated spheres. The outer diameter of each coated sphere was arbitrarily set to 6 μm and the coating thickness was taken as 0, 100, or 200 nm. The refractive indices of the nonabsorbing core and coating were assumed to be 1.4 and 1.6, respectively. The effect of cell wall measured experimentally was also observed in the computed phase function of coated spheres in water. More recently, Kandilian *et al.* [24] compared the experimentally measured and theoretically predicted spectral radiation characteristics of polydisperse green microalgae *C. reinhardtii* grown under nitrogen-replete and nitrogen-limited conditions in the PAR region. The authors showed that the volume-equivalent homogeneous sphere approximation with effective optical properties $n_{\mathrm{eff},\lambda}$ and $k_{\mathrm{eff},\lambda}$, estimated using the expressions proposed by Dauchet *et al.* [22], led to relatively good agreement with measured spectral integral radiation characteristics of polydisperse *C. reinhardtii* cells. Conversely, for polydisperse *C. vulgaris* cells, featuring a thick and strongly refracting cell wall [26,27], the coated sphere approximation for (i) a nonabsorbing coating with the same thickness and constant refractive index as the cell wall and (ii) a core with spectral effective optical properties, also predicted based on [22], led to better agreement with the measured spectral integral radiation characteristics.

Overall, previous studies were based on the assumption that a eukaryotic microalgae cell, by nature heterogeneous, can be approximated by either a homogeneous or coated sphere for the purpose of predicting their radiation characteristics. However, this assumption was never proved or disproved. Thus, it remained unclear whether and under what conditions a heterogeneous eukaryotic microalgae cell consisting of various

intracellular compartments can be approximated as a volume-equivalent homogeneous sphere with some effective optical properties for predicting their spectral radiation characteristics over the PAR region. This study aims to address this question by simulating the heterogeneous nature of spherical microalgae using the T-matrix method and by representing them as a spherical cell with various spherical intracellular compartments having their own optical properties. It also aims to assess theoretically the effect of the intracellular lipid and/or starch accumulation in a cell, due to nitrogen starvation, as well as the effect of the strongly refracting cell wall observed in some species.

2. ANALYSIS

A. Problem Statement

Let us consider a eukaryotic microalgae cell, such as *Chlamydomonas reinhardtii*, composed of a cell wall and various intracellular compartments, including the cytoplasm, chloroplast, nucleus, and mitochondria. In addition, metabolites such as lipid and starch bodies synthesized by the microalgae cell during nitrogen starvation could constitute additional compartments [28].
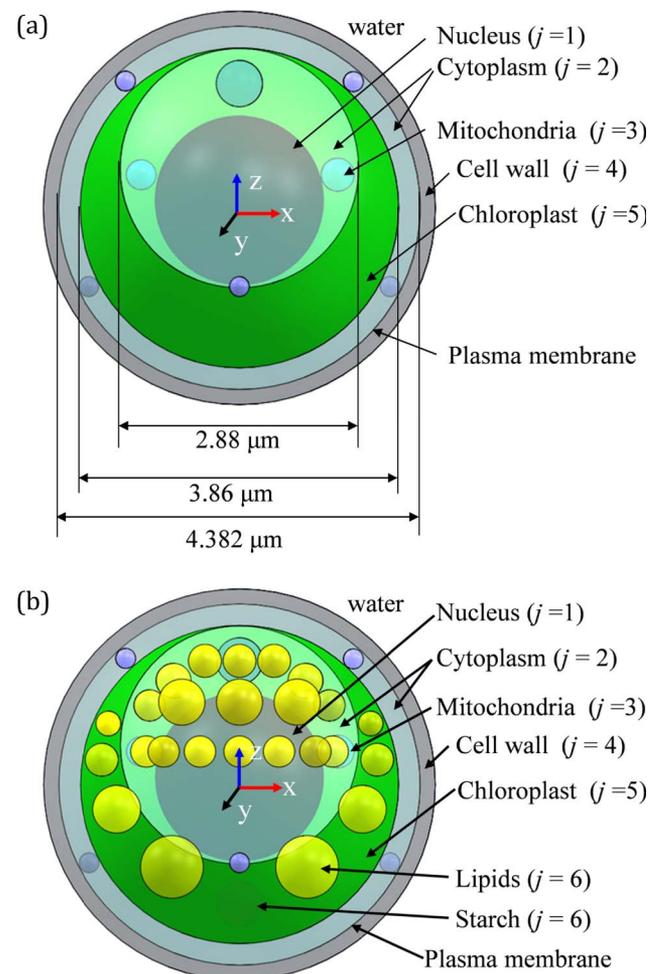
Fig. 1. Schematic of idealized three-dimensional models of heterogeneous quasi-spherical eukaryotic microalgae cell *C. reinhardtii* (a) without metabolites and (b) with metabolites, consisting of spherical intracellular compartments corresponding to various organelles.

Figure 1 depicts schematics of the simulated idealized three-dimensional models of *C. reinhardtii* (a) without and (b) with metabolites. The nucleus ($j = 1$) was represented by a single spherical compartment. The cytoplasm ($j = 2$) was divided into an inner and an outer compartments. Mitochondria ($j = 3$) were represented by nine spherical compartments located within either compartment of the cytoplasm. The cell wall ($j = 4$) was represented by two concentric spheres separated by a distance $t_4 = 184$ nm. In general, the wall thickness of *C. reinhardtii* could vary from 100 to 440 nm [25]. The chloroplast ($j = 5$) was represented by the volume (cup-shaped structure) sandwiched between the inner and outer spherical compartments of the cytoplasm.

Note that the surfaces of all the internal spherical compartments shown in Fig. 1 were nontouching. The volumes of lipids and starch were assumed to be zero under nitrogen-replete conditions and nonzero under nitrogen-limited conditions. These metabolites ($j = 6$) were randomly located in both cytoplasm and chloroplast [29] and the volumes of the cytoplasm and chloroplast were adjusted accordingly. Table 1 summarizes the radius r_j, number of spheres N_j, total volume V_j, and real $n_{j,\lambda}$ and imaginary $k_{j,\lambda}$ parts of the complex index of refraction of each intracellular organelles constituting the idealized heterogeneous cell. Here, the total volume V_j was based on the geometric details reported in the literature [30] and their optical properties were taken from [1,19,31,32].

On the other hand, Table 2 summarizes the range of radius r_6, number of spheres N_6, and the total volume V_6 of lipid compartments, as well as the Chl *a*, chlorophyll *b* (Chl *b*), and photoprotective carotenoid (PPC) concentrations in the simulated microalgae grown under nitrogen-replete and at two different times after sudden nitrogen starvation, namely 12 and 24 h. Indeed, when subjected to nitrogen starvation, *C. reinhardtii* and other microalgae (e.g., *N. oculata*) reduce their pigment concentration Chl *a*, Chl *b*, and PPC concentrations and simultaneously increase their lipid content

[5,6,24,28,33]. Here, each pigment concentration was reduced, from their values under nitrogen-replete conditions, by the same proportions as those observed experimentally for *N. oculata* [6]. The volume fraction of metabolites was taken as 4.2 vol. % after 12 h of nitrogen starvation and as 9.5 vol. % after 24 h. The total volume of metabolites V_6 within a microalgae cell grown under nitrogen-limited conditions was distributed between the cytoplasm and the chloroplast [29] in 74 to 104 spherical droplets having a radius ranging from 150 to 380 nm. This number of spherical lipid droplets, their radius and locations were selected arbitrarily in order to accommodate the total volume of lipids within the volume of cytoplasm and chloroplast. All geometric parameters and coordinates of the different spherical compartments are available in digital form in an Excel spreadsheet [34].

The medium surrounding the cell was nonabsorbing with refractive index n_m taken as constant and equal to 1.333, corresponding to that of water [35]. All compartments other than the chloroplast were nonabsorbing (i.e., $k_{j,\lambda} = 0$ for $j = 1, 2, 3, 4, 6$) with different refractive indices $n_{j,\lambda}$ taken from the literature [1,19,32] and given in Table 1. The refractive index $n_{5,\lambda}$ of the chloroplast ($j = 5$) was assumed to be constant and equal to 1.42 over the PAR region [31]. However, the chloroplast absorption index $k_{5,\lambda}$ depended on the pigment concentrations C_i (in kg/m³) and on their specific spectral absorption coefficients $Ea_{i,\lambda}(\lambda)$ (in m²/kg) according to [16]

$$k_{5,\lambda} = \frac{\lambda}{4\pi} \sum_{i=1}^{M} Ea_{i,\lambda}(\lambda) C_i = \frac{\lambda}{4\pi} \rho_{dm} \left(\frac{1 - x_w}{x_w} \right) \sum_{i=1}^{M} Ea_{i,\lambda}(\lambda) w_i,$$

(1)

where the index i refers to one of the M pigments present in the chloroplast. The concentration C_i of pigment i can be expressed in terms of its mass fraction w_i, the density of dry material ρ_{dm} (in kg/m³), and the *in vivo* volume fraction of water in the cell x_w. The specific spectral absorption coefficient

Table 1. Radius r_j, Number of Spheres N_j, Total Volume V_j, and Real $n_{j,\lambda}$ and Imaginary $k_{j,\lambda}$ Parts of the Complex Index of Refraction of Various Intracellular Organelles as Well as Metabolites of a Representative Eukaryotic Microalgae Cell of Radius $r_c = 2.375$ μm

Compartments	j	r_j (μm)	N_j	V_j (μm³)	$n_{j,\lambda}$	$k_{j,\lambda}$
Nucleus	1	1.018	1	4.42[b]	1.38[a]	0
Mitochondria	2	0.12–0.28	9	0.193[d]	1.38[a]	0
Cytoplasm	3	—	1	21.967[d]	1.36[c]	0
Cell (including cell wall)	4	2.375	1	56.08[b]	1.375[e]	0
Chloroplast	5	—	2	17.50[b]	1.42[c]	Eq. (1)
Lipid bodies	6	—	—	0	1.49[d]	0
Starch	6	—	—	0	1.51[d]	0

[a][19], [b][30], [c][31], [d]assumed, and [e][32]

Table 2. Radius r_6, Number of Spheres N_6, and Total Volume V_6 of Lipid Bodies, Chl *a*, Chl *b*, and PPC Concentrations of Cell Grown under Nitrogen-Replete and Nitrogen-Limited Conditions

Growth condition	Time (hr)	r_6 (μm)	N_6	V_6 (μm³)	Chl *a* (wt. %)	Chl *b* (wt. %)	PPC (wt. %)
Nitrogen-replete	—	0	0	0	5.58	2.79	1.79
Nitrogen-limited	12	0.15–0.28	78	2.36	3.45	1.73	1.43
	24	0.15–0.38	104	5.30	2.14	1.07	1.10

$Ea_{i,\lambda}(\lambda)$ of pigment i corresponding to Chl a, Chl b, and PPC was reported by Bidigare *et al.* [36]. The value of each pigment mass fraction $w_{\text{pig},i}$ and *in vivo* water volume fraction x_w in the cell were taken as those of *C. reinhardtii* reported by Pottier *et al.* [16] (Table 2). On the other hand, the density of dry material ρ_{dm} was considered to be 1400 kg/m^3 [24] while the water volume fraction in the cell x_w was taken as 0.78 [16]. The main structural component of the cell wall of *C. reinhardtii* is hydroxyproline rich glycoprotein [37] whose refractive index $n_{4,\lambda}$ in the visible wavelength was reported as 1.375 [32].

B. Prediction of Spectral Radiation Characteristics of a Heterogeneous Cell

The orientation-averaged spectral absorption $\langle C_{\text{abs},\lambda} \rangle$ and scattering $\langle C_{\text{sca},\lambda} \rangle$ cross sections of the spherical heterogeneous eukaryotic cell models (Fig. 1) were evaluated using the multiple sphere superposition T-matrix code for multiple internal sphere situations developed by Mackowski [38]. The superposition T-matrix method estimates the scattered electromagnetic (EM) field from overall heterogeneous spheres by superposing the scattered EM fields from each of the constituting spherical compartments [39]. The method uses an analytical rotation transformation rule to integrate the incident EM field over every propagation direction. Then, the orientation-averaged scattering $\langle Q_{\text{sca},\lambda} \rangle$ and extinction $\langle Q_{\text{ext},\lambda} \rangle$ efficiency factors, and the normalized Stokes scattering matrix elements $[F_{ij}(\Theta)]$ of the randomly oriented multisphere structure can be obtained from operations on the T-matrix [39]. On the other hand, the orientation-averaged absorption efficiency factor can be evaluated as $\langle Q_{\text{abs},\lambda} \rangle = \langle Q_{\text{ext},\lambda} \rangle - \langle Q_{\text{sca},\lambda} \rangle$. Next, the orientation-averaged absorption and scattering cross sections of the heterogeneous cell were calculated from the computed absorption $\langle Q_{\text{abs},\lambda} \rangle$ and scattering $\langle Q_{\text{sca},\lambda} \rangle$ efficiency factors according to [40]

$$\langle C_{\text{abs/sca},\lambda} \rangle = \langle Q_{\text{abs/sca},\lambda} \rangle \pi r_c^2, \tag{2}$$

where r_c is the radius of the entire cell, including the cell wall. In addition, the asymmetry factor and the single scattering albedo were, respectively, defined as [40]

$$g_\lambda = \frac{1}{2} \int_0^\pi \Phi_\lambda(\theta) \sin \theta \cos \theta d\theta \quad \text{and} \quad \omega_\lambda = \langle Q_{\text{sca},\lambda} \rangle / \langle Q_{\text{ext},\lambda} \rangle, \tag{3}$$

where $\Phi_\lambda(\theta)$ is the azimuthally symmetric orientation-averaged scattering phase function, which depends only on the polar angle θ varying from 0° to 180°. Then, the backscattering ratio, denoted by b_λ, is defined as [16]

$$b_\lambda = \frac{1}{2} \int_{\pi/2}^\pi \Phi_\lambda(\theta) \sin \theta d\theta, \tag{4}$$

while the orientation-averaged backscattering cross section $\langle C_{\text{back},\lambda} \rangle$ is expressed as [41]

$$\langle C_{\text{back},\lambda} \rangle = b_\lambda \langle C_{\text{sca},\lambda} \rangle. \tag{5}$$

C. Volume-Equivalent Homogeneous Sphere with Some Effective Optical Properties

The heterogeneous cell was approximated as a volume-equivalent homogeneous sphere having radius r_c and effective complex index of refraction denoted by $m_{\text{eff},\lambda} = n_{\text{eff},\lambda} + ik_{\text{eff},\lambda}$. The

effective refractive $n_{\text{eff},\lambda}$ and absorption $k_{\text{eff},\lambda}$ indices were defined as a weighted sum of the refractive $n_{j,\lambda}$ and absorption $k_{j,\lambda}$ indices of the six different cell compartments according to [1]

$$n_{\text{eff},\lambda} = \sum_{j=1}^{6} n_{j,\lambda} f_{v,j} \quad \text{and} \quad k_{\text{eff},\lambda} = \sum_{j=1}^{6} k_{j,\lambda} f_{v,j}, \tag{6}$$

where $f_{v,j}$ is the volume fraction of the cellular compartment, such that $f_{v,j} = V_j / V_c$ with V_c being the total cell volume, i.e., $V_c = 4\pi r_c^3 / 3$. Here, $k_{\text{eff},\lambda}$ varied with wavelength through $k_{5,\lambda}$ while $n_{\text{eff},\lambda}$ was constant over the PAR region. Then, the radiation characteristics of the volume-equivalent homogeneous sphere were computed using a program based on the Lorenz–Mie theory developed by Matzler [42]. Note that this study considered volume averaging of the complex refractive indices of the different constituents of the heterogeneous cells for its simple formulation for heterogeneous cells. Indeed, it was not clear how to implement the numerous and widely used two-phase effective medium approximations (e.g., Maxwell–Garnett theory, Drude, symmetric and nonsymmetric Bruggeman's models) to such multiphase systems [43].

D. Coated Sphere Approximation

The heterogeneous cell was also approximated as a coated sphere with an outer radius identical to that of the cell r_c and an inner core of radius r_{core} ($= r_c - t_4$) encompassing all the intracellular compartments. The core effective spectral refractive $n_{\text{core},\lambda}$ and absorption $k_{\text{core},\lambda}$ indices were estimated based on Eq. (6) but excluding the cell wall ($j = 4$) in the summation. The volume fraction of each compartment in the core was expressed as $f_{v,c} = V_j / V_{\text{core}}$, where V_{core} is the volume of the core, i.e., $V_{\text{core}} = 4\pi r_{\text{core}}^3 / 3$. On the other hand, the refractive and absorption indices of coating were that of the wall, i.e., $n_{\text{coat},\lambda} = n_{4,\lambda} = 1.375$ and $k_{\text{coat},\lambda} = k_{4,\lambda} = 0$. Here also, the absorption and scattering cross sections for the equivalent coated sphere were evaluated using Lorenz–Mie theory [42].

3. RESULTS AND DISCUSSION

A. Radiation Characteristics of Microalgae Cell Grown under Stress

Figure 2 depicts the orientation-averaged spectral (a) absorption $\langle C_{\text{abs},\lambda} \rangle$ and (b) scattering $\langle C_{\text{sca},\lambda} \rangle$ cross sections, (c) scattering phase function $\Phi_{634}(\theta)$ at wavelength 634 nm, and (d) the spectral backscattering ratio b_λ in the PAR region for the heterogeneous eukaryotic microalgae cell composed of a weakly refracting wall ($n_{4,\lambda} = 1.375$) and grown under nitrogen-replete and nitrogen-limited conditions. The optical properties of all other intracellular compartments were kept the same as those reported in Table 1 while the pigment concentrations corresponding to nitrogen-replete and nitrogen-limited conditions and necessary to estimate $k_{5,\lambda}$ [Eq. (1)] were given in Table 2. Figure 2 also compares the radiation characteristics of the heterogeneous cell with those of the volume-equivalent homogeneous sphere and coated sphere approximations previously described.

First, Fig. 2(a) reveals that the absorption cross section $\langle C_{\text{abs},\lambda} \rangle$ of all simulated microalgae cells featured absorption peaks corresponding to those of the chlorophyll a (around
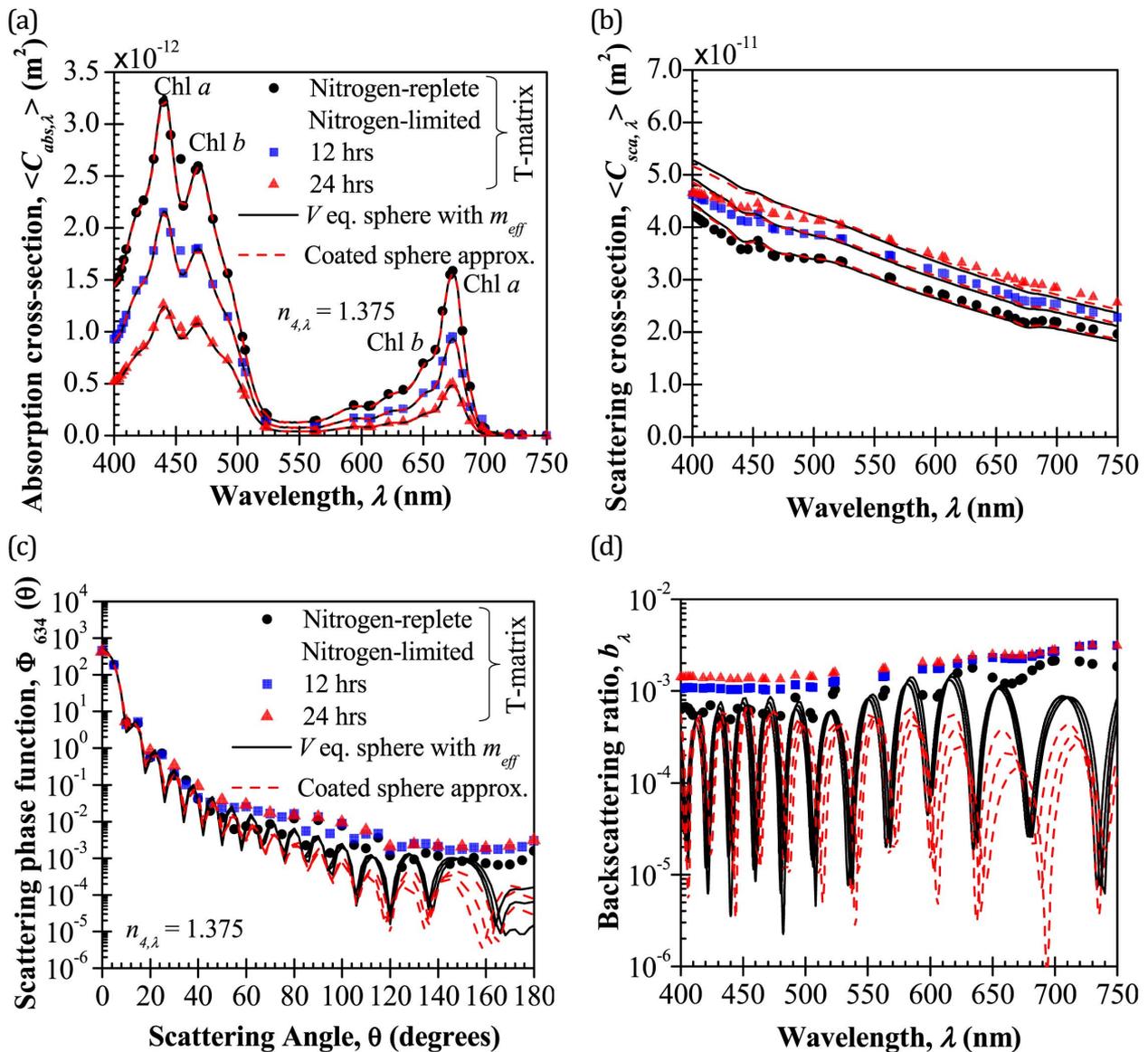
Fig. 2. Comparison between the estimated spectral (a) absorption cross section $\langle C_{abs,\lambda} \rangle$, (b) scattering cross section $\langle C_{sca,\lambda} \rangle$, (c) scattering phase function $\Phi_{634}(\theta)$ at wavelength 634 nm, and (d) spectral backscattering ratio b_λ of heterogeneous eukaryotic microalage cell with wall refractive indices $n_{4,\lambda} = 1.375$ grown under nitrogen-replete conditions, and after 12 and 24 h of nitrogen-limited conditions, and those correspond to the simplified approximations.

435 and 676 nm) and chlorophyll b (around 475 and 650 nm) [36]. Both pigments were present in the chloroplast and were accounted for in the expression of $k_{5,\lambda}$ given by Eq. (1). In addition, the order of magnitude of $\langle C_{abs,\lambda} \rangle$ predicted was similar to that measured experimentally for *N. oculata* 1.5–3.5 μm in diameter [5,6]. Figure 2(a) also shows that the spectral absorption cross section $\langle C_{abs,\lambda} \rangle$ of the cell grown under nitrogen-limited conditions was smaller than that of the cell grown under nitrogen-replete conditions and decreased with time due to the decrease in pigment concentrations associated with the increase in lipid content (Table 2). These observations are consistent with experimental measurements for *N. oculata* [5] and *Anabaena cylindrica* [44]. Moreover, the predictions of the spectral absorption cross section $\langle C_{abs,\lambda} \rangle$ by the volume-equivalent homogeneous sphere and the coated sphere approximations were

in excellent agreement (within 5%) with those by the superposition T-matrix method for all growth conditions considered.

Figure 2(b) demonstrates that the scattering cross section $\langle C_{sca,\lambda} \rangle$ of the cell grown under nitrogen-limited conditions was larger than that of the cell grown under nitrogen-replete conditions. This was also consistent with experimental measurements [5]. It can be attributed to (i) the reduction in absorption by pigments and (ii) the increase in volume fraction of metabolites featuring larger refractive index $n_{6,\lambda}$ than other intracellular compartments (Tables 1 and 2). Moreover, scattering dominated over absorption. In fact, the single-scattering albedo was larger than 0.9 across the PAR region for all growth conditions considered. Also, the spectral scattering cross section $\langle C_{sca,\lambda} \rangle$ estimated using the volume-equivalent homogeneous sphere and the coated sphere approximations

agreed well with the predictions by the superposition T-matrix method. In fact, the associated PAR-averaged relative difference was less than 6% for all growth conditions considered. However, the maximum relative error increased to 14% as the volume of metabolite increased, particularly for a wavelength less than 500 nm.

Figure 2(c) shows that the scattering phase function $\Phi_{634}(\theta)$ was strongly peaked in forward directions for all growth conditions considered. This was due to the large cell size parameter and consistent with the measured scattering phase function for a wide range of microalgae cells and growth conditions [20,45]. In addition, the scattering phase function $\Phi_{634}(\theta)$ of the microalgae cell grown under nitrogen-limited conditions was larger than that for nitrogen-replete conditions for a scattering angle larger than 50°. This can be attributed to the larger number of refracting metabolite compartments in the cell under nitrogen limitation. This reveals that the internal structures of a microalgae cell have great influence on light scattering, particularly in the backward directions. This was also observed experimentally by Volten *et al.* [45] for three *Microcystis* samples featuring different volume fractions of gas vacuoles. Moreover, for forward scattering angle θ less than 10°, the scattering phase function predicted by the homogeneous and coated sphere approximations was in good agreement with predictions by the T-matrix method for the heterogeneous cell. In these forward directions, scattering was dominated by diffraction and predictions were not affected significantly by the choice of the model. However, for scattering angle θ larger than 20° the scattering phase function $\Phi_{634}(\theta)$ predicted by both approximations featured strong resonances that were not observed in the scattering phase function of the heterogeneous cell. This can be attributed to the fact that closely packed heterogeneities destroyed the resonances observed in a homogeneous sphere and a coated sphere resulting in a quasi-monotonic phase function [18,19,24,25,45,46]. This phenomenon was also observed theoretically for a purely scattering heterogeneous spherical cell with either spherical organelles [18] or nonspherical organelles [19].

Figure 2(d) illustrates that backscattering by the heterogeneous cell increases with an increase in volume fraction of metabolites. The presence of a large number of metabolites within the cell led to a smooth b_λ over the PAR region compared with that of the cell without metabolites. In addition, both volume-equivalent homogeneous sphere and coated sphere approximations underestimated the spectral backscattering ratio b_λ across the PAR region under all growth conditions. These approximations were not appropriate for estimating scattering phase function and the spectral backscattering ratio of a heterogeneous microalgae cell. Similar conclusions were reached experimentally with various phytoplanktons [45,47].

B. Radiation Characteristics of Microalgae Cells with Weakly and Strongly Refracting Walls

Figure 3 depicts the orientation-averaged spectral (a) absorption $\langle C_{abs,\lambda} \rangle$ and (b) scattering $\langle C_{sca,\lambda} \rangle$ cross sections, (c) the scattering phase function $\Phi_{634}(\theta)$ at wavelength 634 nm, and (d) the spectral backscattering ratio b_λ of heterogeneous microalgae cells grown under nitrogen-replete conditions but composed of either a weakly ($n_{4,\lambda} = 1.375$) or a strongly ($n_{4,\lambda} = 1.5$) refracting wall. Figure 3 also compares the

radiation characteristics of a heterogeneous cell in the PAR region with those of the corresponding volume-equivalent homogeneous sphere and coated sphere approximations.

First, Fig. 3(a) indicates that both cells had nearly identical absorption cross section $\langle C_{abs,\lambda} \rangle$ despite the fact that one of them had a highly refracting wall. In addition, the estimated absorption cross section of heterogeneous cells with weakly and strongly refracting walls predicted by the T-matrix method displayed similar peaks and valleys as that of the measured mass absorption cross sections of *C. reinhardtii* [4] and *Chlorella sp.* [48] cells in the PAR region. Finally, the absorption cross section $\langle C_{abs,\lambda} \rangle$ of two types of cells estimated using the volume-equivalent homogeneous sphere and the coated sphere approximations was in very good agreement with predictions by the superposition T-matrix method, with a maximum relative difference less than 5% and 4%, respectively.

Figure 3(b) demonstrates that for identical wall thickness, the cell with the strongly refracting wall ($n_{4,\lambda} = 1.5$) scattered light more than the cell with the weakly refracting wall ($n_{4,\lambda} = 1.375$) due to the greater mismatch in refractive index with the surrounding medium. Furthermore, it is evident from Figs. 2(b) and 3(b) that the effect of mismatch in the refractive index of the cell wall has great influence on the scattering cross section of a heterogeneous cell grown under nitrogen-replete conditions in comparison to the effect of intracellular compartments. Finally, the spectral scattering cross section $\langle C_{sca,\lambda} \rangle$ of two types of microalgae cell revealed resonances corresponding to chlorophyll *a* and *b* absorption peak. Moreover, this figure also revealed that the volume-equivalent homogeneous sphere approximation failed to predict $\langle C_{sca,\lambda} \rangle$ accurately for the heterogeneous cell with a strongly refracting wall ($n_{4,\lambda} = 1.5$). However, in this case, predictions by the coated sphere approximation were in good agreement with those obtained by the superposition T-matrix method, with a maximum relative difference less than 6%.

Figure 3(c) shows that the scattering phase function $\Phi_{634}(\theta)$ of a heterogeneous cell with a strongly refracting wall ($n_{4,\lambda} = 1.5$) was larger than that for a cell with a weakly refracting wall ($n_{4,\lambda} = 1.375$) for a scattering angle greater than 10° and even more prominently in the backward directions. This was mainly due to greater mismatch in the refractive index between the cell wall and the surrounding medium. These observations were consistent with (a) *in situ* measurement of concentrated *C. vulgaris* cells in growth medium compared to that of the concentrated *C. reinhardtii* cells [24], and (b) theoretical study on polydisperse three-layered spherical cells [49].

Figure 3(d) shows the spectral backscattering ratio b_λ over the PAR region. It indicates that b_λ was highly sensitive to the refractive index of the cell wall. Here also, the scattering phase function $\Phi_{634}(\theta)$ [Fig. 3(c)] and the spectral backscattering ratio b_λ [Fig. 3(d)] predicted by the homogeneous sphere and coated sphere approximations featured strong resonances which were not observed with the heterogeneous cell. This can be attributed to the fact that, for the replete conditions simulated, the number of intracellular components was relatively small, and were widely spaced. As a result, resonances, albeit weak, appeared in $\Phi_{634}(\theta)$ and b_λ. Such resonances were observed for cells with a large number of metabolites [Figs. 2(c) and
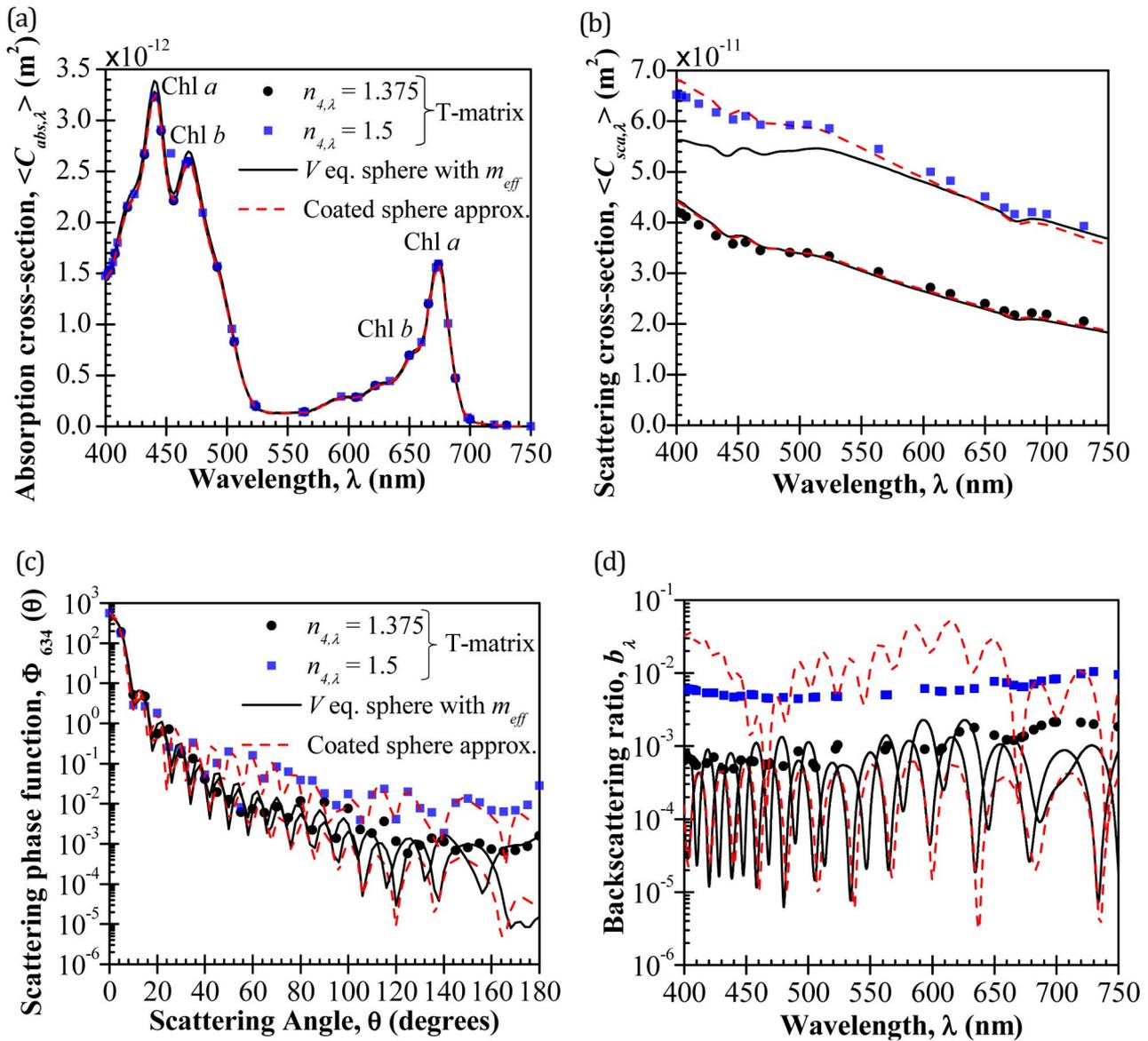
Fig. 3. Comparison between the estimated spectral (a) absorption cross section $\langle C_{abs,\lambda} \rangle$, (b) scattering cross section $\langle C_{sca,\lambda} \rangle$, (c) scattering phase function $\Phi_{634}(\theta)$ at wavelength 634 nm, and (d) spectral backscattering ratio b_λ of heterogeneous eukaryotic microalage cells with wall refractive indices $n_{4,\lambda} = 1.375$ and 1.5 and those from homogeneous and coated sphere approximations.

2(d)]. Finally, the homogeneous sphere approximation under-estimated the scattering phase function $\Phi_{634}(\theta)$ for $\theta > 40°$ and the spectral backscattering ratio b_λ, for the heterogeneous cell with a strongly refracting wall ($n_{4,\lambda} = 1.5$). On the other hand, the coated sphere approximation led to somewhat better agreement in $\Phi_{634}(\theta)$ and b_λ.

Overall, the above results revealed that both homogeneous and coated sphere approximations were inappropriate for estimating the scattering phase function and the spectral backscattering ratio of a heterogeneous cell with a strongly refracting wall. However, the coated sphere approximation could accurately predict the spectral absorption and scattering cross sections, the spectral asymmetry factor, and the spectral scattering albedo of a heterogeneous microalgae cell with a strongly refracting wall. These results were consistent with recent experimental measurements of the integral radiation characteristics

and scattering phase function of *C. reinhardtii* and *C. vulgaris* cells under replete or nitrogen-limited conditions [24].

4. CONCLUSION

This study estimated the spectral absorption and scattering cross section, the scattering phase function, and the spectral backscattering ratio, in the PAR region, of randomly oriented spherical heterogeneous eukaryotic microalgae cells enclosing various spherical intracellular organelles using the T-matrix method. The predicted orientation-averaged spectral absorption cross section of heterogeneous cells was found to be consistent with those measured experimentally and featured absorption peaks corresponding to those of Chl a and Chl b. The absorption cross section also decreased for the cells with a simultaneous increase in the fraction of metabolites and

decrease in pigment concentrations caused by nitrogen-limited conditions. On the other hand, their scattering cross section increased across the PAR region. Furthermore, the cell with a strongly refracting wall displayed a large scattering cross section compared with the cell with a weakly refracting wall. Moreover, all types of cells displayed a strong peak in the phase function in the forward directions. However, the strongly refracting wall resulted in stronger backscattering. Overall, the simulation results for a single heterogeneous cell were qualitatively and quantitatively consistent with recent experimental measurements [24,45].

Moreover, the volume-equivalent homogeneous sphere approximation with volume-averaged effective optical properties gave good predictions of the absorption and scattering cross sections of the heterogeneous microalgae cell with a weakly refracting wall grown under nitrogen-replete and nitrogen-limited conditions. However, for the cell with a strongly refracting wall, the coated sphere approximation featuring a coating representing the cell wall and a homogeneous core with volume-averaged complex index of refraction representing the intracellular compartments led to better predictions of the integral radiation characteristics. Finally, both approximations failed to accurately predict the scattering phase function and the spectral backscattering ratio and featured strong resonances that were not observed for the heterogeneous cell.

REFERENCES

1. M. Jonasz and G. R. Fournier, *Light Scattering by Particles in Water* (Academic, 2007).
2. A. Bricaud and A. Morel, "Light attenuation and scattering by phytoplanktonic cells: a theoretical modeling," Appl. Opt. **25**, 571–580 (1986).
3. A. Bricaud, A. L. Bédhomme, and A. Morel, "Optical properties of diverse phytoplanktonic species: Experimental results and theoretical interpretation," J. Plankton Res. **10**, 851–873 (1988).
4. H. Berberoğlu, L. Pilon, and A. Melis, "Radiation characteristics of *Chlamydomonas reinhardtii* CC125 and its truncated chlorophyll antenna transformants *tla1, tlaX* and *tla1-CW+*," Int. J. Hydrogen Energy **33**, 6467–6483 (2008).
5. R. L. Heng and L. Pilon, "Time-dependent radiation characteristics of *Nannochloropsis oculata* during batch culture," J. Quant. Spectrosc. Radiat. Transfer **144**, 154–163 (2014).
6. R. Kandilian, J. Pruvost, J. Legrand, and L. Pilon, "Influence of light absorption rate by *Nannochloropsis oculata* on triglyceride production during nitrogen starvation," Bioresour. Technol. **163**, 308–319 (2014).
7. A. Sukenik, R. S. Levy, Y. Levy, P. G. Falkowski, and Z. Dubinsky, "Optimizing algal biomass production in an outdoor pond: a simulation model," J. Appl. Phycol. **3**, 191–201 (1991).
8. S. Sathyendranath, G. Cota, V. Stuart, H. Maass, and T. Platt, "Remote sensing of phytoplankton pigments: a comparison of empirical and theoretical approaches," Int. J. Remote Sens. **22**, 249–273 (2001).
9. A. Morel and S. Maritorena, "Bio-optical properties of oceanic waters—A reappraisal," J. Geophys. Res. **106**, 7163–7180 (2001).
10. J. E. O'Reilly, S. Maritorena, D. A. Siegel, M. C. O'Brien, D. Toole, F. P. Chavez, P. Strutten, G. F. Cota, S. B. Hooker, C. R. McClain, K. L. Carder, F. Muller-Karger, L. Harding, A. Magnuson, D. Phinney, G. F. Moore, J. Aiken, K. R. Arrigo, R. Letelier, and M. Culver, "Ocean chlorophyll-a algorithms for SeaWiFS, OC2 and OC4: version 4," in *SeaWiFS Postlaunch Calibration and Validation Analyses: Part 3. NASA Tech. Memo. 2000-206892*, S. B. Hooker and E. R. Firestone, eds. (NASA Goddard Space Flight Center, 2000), Vol. **11**, pp. 9–23.
11. P. J. L. B. Williams and L. M. Laurens, "Microalgae as biodiesel & biomass feedstocks: review and analysis of the biochemistry, energetics & economics," Energy Environ. Sci. **3**, 554–590 (2010).
12. L. Pilon and H. Berberoğlu, "Photobiological hydrogen production," in *Handbook of Hydrogen Energy*, S. A. Sherif, D. Y. Goswami, E. K. Stefanakos, and A. Steinfeld, eds. (CRC Press, 2014), Chap. 11, pp. 369–418.
13. M. J. Barbosa, J. Hoogakker, and R. H. Wijffels, "Optimisation of cultivation parameters in photobioreactors for microalgae cultivation using the A-stat technique," Biomol. Eng. **20**, 115–123 (2003).
14. R. Kandilian, T. C. Tsao, and L. Pilon, "Control of incident irradiance on a batch operated flat-plate photobioreactor," Chem. Eng. Sci. **119**, 99–108 (2014).
15. J. F. Cornet, C. G. Dussap, J. B. Gros, C. Binois, and C. Lasseur, "A simplified monodimensional approach for modeling coupling between radiant light transfer and growth kinetics in photobioreactors," Chem. Eng. Sci. **50**, 1489–1500 (1995).
16. L. Pottier, J. Pruvost, J. Deremetz, J. F. Cornet, J. Legrand, and C. G. Dussap, "A fully predictive model for one-dimensional light attenuation by *Chlamydomonas reinhardtii* in a torus photobioreactor," Biotechnol. Bioeng. **91**, 569–582 (2005).
17. H. Takache, J. Pruvost, and J. F. Cornet, "Kinetic modeling of the photosynthetic growth of *Chlamydomonas reinhardtii* in a photobioreactor," Biotechnol. Prog. **28**, 681–692 (2012).
18. G. Videen and D. Ngo, "Light scattering multipole solution for a cell," J. Biomed. Opt. **3**, 212–220 (1998).
19. R. Drezek, A. Dunn, and R. Richards-Kortum, "Light scattering from cells: finite-difference time-domain simulations and goniometric measurements," Appl. Opt. **38**, 3651–3661 (1999).
20. L. Pilon and R. Kandilian, "Interaction between light and photosynthetic microorganisms," in *Advances in Chemical Engineering*, J. Legrand, ed. (Elsevier, 2016), Vol. **46**, Chap. 2, pp. 107–149.
21. A. Quirantes and S. Bernard, "Light-scattering methods for modelling algal particles as a collection of coated and/or nonspherical scatterers," J. Quant. Spectrosc. Radiat. Transfer **100**, 315–324 (2006).
22. J. Dauchet, S. Blanco, J. F. Cornet, and R. Fournier, "Calculation of the radiative properties of photosynthetic microorganisms," J. Quant. Spectrosc. Radiat. Transfer **161**, 60–84 (2015).
23. E. Lee, R. L. Heng, and L. Pilon, "Spectral optical properties of selected photosynthetic microalgae producing biofuels," J. Quant. Spectrosc. Radiat. Transfer **114**, 122–135 (2013).
24. R. Kandilian, J. Pruvost, A. Artu, C. Lemasson, J. Legrand, and L. Pilon, "Comparison of experimentally and theoretically determined radiation characteristics of photosynthetic microorganisms," J. Quant. Spectrosc. Radiat. Transfer **175**, 30–45 (2016).
25. Ø. Svensen, Ø. Frette, and S. R. Erga, "Scattering properties of microalgae: the effect of cell size and cell wall," Appl. Opt. **46**, 5762–5769 (2007).
26. H. G. Geken, B. Donohoe, and E. P. Knoshaug, "Enzymatic cell wall degradation of *Chlorella vulgaris* and other microalgae for biofuels production," Planta **237**, 239–253 (2013).
27. A. W. Atkinson, B. E. S. Gunning, and P. C. L. John, "Sporopollenin in the cell wall of *Chlorella* and other algae: ultrastructure, chemistry, and incorporation of 14C-acetate, studied in synchronous cultures," Planta **107**, 1–32 (1972).
28. A. E. Solovchenko, "Physiological role of neutral lipid accumulation in eukaryotic microalgae under stresses," Russ. J. Plant Physiol. **59**, 167–176 (2012).
29. C. Goodson, R. Roth, Z. T. Wang, and U. Goodenough, "Structural correlates of cytoplasmic and chloroplast lipid body synthesis in *Chlamydomonas reinhardtii* and stimulation of lipid body production with acetate boost," Eukaryot. Cell **10**, 1592–1606 (2011).
30. F. Schötz, H. Bathelt, C. G. Arnold, and O. Schimmer, "The architecture and organization of the *Chlamydomonas* cell. Results of

serial-section electron microscopy and a three-dimensional reconstruction," Protoplasma **75**, 229–254 (1972).

31. E. Charney and F. S. Brackett, "The spectral dependence of scattering from a spherical alga and its implications for the state of organization of the light-accepting pigments," Arch. Biochem. Biophys. **92**, 1–12 (1961).

32. M. M. Brysk and M. J. Chrispeels, "Isolation and partial characterization of a hydroxyproline-rich cell wall glycoprotein and its cytoplasmic precursor," Biochim. Biophys. Acta, Protein Struct. **257**, 421–432 (1972).

33. Z. T. Wang, N. Ullrich, S. Joo, S. Waffenschmidt, and U. Goodenough, "Algal lipid bodies: stress induction, purification, and biochemical characterization in wild-type and starchless *Chlamydomonas reinhardtii*," Eukaryot. Cell **8**, 1856–1868 (2009).

34. https://github.com/arkabhowmik2656/Cell_coordinates.

35. G. M. Hale and M. R. Querry, "Optical constants of water in the 200-nm to 200-μm wavelength region," Appl. Opt. **12**, 555–563 (1973).

36. R. R. Bidigare, M. E. Ondrusek, J. H. Morrow, and D. A. Kiefer, "*In-vivo* absorption properties of algal pigments," Proc. SPIE **1320**, 290–302 (1990).

37. J. W. Catt, G. J. Hills, and K. Roberts, "Cell wall glycoproteins from *Chlamydomonas reinhardii*, and their self-assembly," Planta **138**, 91–98 (1978).

38. D. W. Mackowski, "A general superposition solution for electromagnetic scattering by multiple spherical domains of optically active media," J. Quant. Spectrosc. Radiat. Transfer **133**, 264–270 (2014).

39. D. W. Mackowski and M. I. Mishchenko, "Calculation of the T-matrix and the scattering matrix for ensembles of spheres," J. Opt. Soc. Am. A **13**, 2266–2278 (1996).

40. K. N. Liou, *An Introduction to Atmospheric Radiation* (Academic, 2002).

41. A. M. Sánchez and J. Piera, "Methods comparison to retrieve the refractive index of small scatterers," Biogeosci. Discuss. **12**, 18723–18768 (2015).

42. C. Mätzler, "MATLAB functions for Mie scattering and absorption," version 2, report no. 2002–11 (Institutfür Angewandte Physik, 2002), http://www.hiwater.org/Mie_calcs.html.

43. N. J. Hutchinson, T. Coquil, A. Navid, and L. Pilon, "Effective optical properties of highly ordered mesoporous thin films," Thin Solid Films **518**, 2141–2146 (2010).

44. R. L. Heng, E. Lee, and L. Pilon, "Radiation characteristics and optical properties of filamentous cyanobacterium *Anabaena cylindrica*," J. Opt. Soc. Am. A **31**, 836–845 (2014).

45. H. Volten, J. F. de Han, J. W. Hovenier, R. Schreurs, W. Vassen, A. G. Dekker, H. J. Hoogenboom, F. Charlton, and R. Wouts, "Laboratory measurements of angular distributions of light scattered by phytoplankton and slit," Limnol. Oceanogr. **43**, 1180–1197 (1998).

46. M. I. Mishchenko and L. Liu, "Morphology-dependent resonances of spherical droplets with numerous microscopic inclusions," Opt. Lett. **39**, 1701–1704 (2014).

47. R. D. Vaillancourt, C. W. Brown, R. R. L. Guillard, and W. M. Balch, "Light backscattering properties of marine phytoplankton: relationships to cell size, chemical composition, and taxanomy," J. Plankton. Res. **26**, 191–212 (2004).

48. H. Berberoğlu, P. S. Gomez, and L. Pilon, "Radiation characteristics of *Botryococcus braunii*, *Chlorococcum littorale*, and *Chlorella sp.* used for CO_2 fixation and biofuel production," J. Quant. Spectrosc. Radiat. Transfer **110**, 1879–1893 (2009).

49. J. C. Kitchen and J. R. V. Zaneveld, "A three-layered sphere model of the optical properties of phytoplankton," Limnol. Oceanogr. **37**, 1680–1690 (1992).